Comparison of Clustering Methods for Crop-Growth Analysis Using Multi-Temporal NDVI: Spectral vs Optics

Srikari Shasi Patel[1], Kuricheti Prerana[1], Sajith Variyar V. V.[1], Ramesh Sivanpillai[2]

[1] Amrita School of Artificial Intelligence, Amrita Vishwa Vidyapeetham, Coimbatore, India
(srikarishasipatel@gmail.com, ORCID: 0009-0002-9420-1702; preranakuricheti18@gmail.com, ORCID: 0009-0004-4581-6182;
vv sajithvariyar@cb.amrita.edu, ORCID: 0000-0003-3944-8155)

[2] Wyoming GIS Center, School of Computing, University of Wyoming, Laramie, WY 82071, USA
(sivan@uwyo.edu, ORCID: 0000-0003-3547-9464)

Keywords: OPTICS, Spectral Clustering, Density-based Clustering, Graph-based clustering, Cluster validation,Machine Learning.

Abstract

The primary objective of this study was to compare the density-based (OPTICS-Ordering Points To Identify the Clustering Structure) and graph-based (Spectral Clustering) algorithms for identifying Normalized Difference Vegetation Index (NDVI) -based crop growth clusters in multi-temporal satellite imagery from two crop fields in southeast Wyoming, USA. The clusters represent spatial groupings of pixels with similar NDVI values, corresponding to relative crop growth and vigor conditions across the fields. This study evaluated the similarities and differences in the clusters generated by these two unsupervised Machine Learning (ML) algorithms. Spectral clustering cannot find the number of clusters, so eigengap was used to estimate the number of optimal clusters. The same number was enforced in OPTICS which used the parameters: min samples, max eps and Xi. OPTICS generated more fragmented and fine-scale clusters, especially in higher NDVI ranges, whereas Spectral Clustering produced smoother, more contiguous zones, particularly in moderate to low NDVI areas. The cluster output images generated by Spectral and OPTICS had only 55% overlap. It showed that OPTICS is better suited when the objective is to detect fine-grained variability in crop vigor, especially in dense vegetation, while Spectral Clustering is more effective for identifying broad growth zones and overall field patterns. The choice of algorithm should therefore depend on whether detailed local differences or generalized field-wide structures are of greater importance.

1. Introduction

Accurate characterization of spatial variability in imagery from satellite is essential for agricultural monitoring and vegetation mapping. Remote sensing is an important tool for evaluating crop growth and irrigation performance in irrigated agricultural systems because spatial variations in vegetation condition frequently reflect differences in water availability, soil properties, and management practices (Atzberger, 2013). The increasing accessibility of multi-temporal and high-resolution satellite data has made machine learning techniques essential for deriving useful insights from massive agricultural datasets.

However, large amounts of labelled training data are needed for many advanced machine learning and deep learning techniques, which are frequently challenging and expensive to acquire in actual agricultural settings. This limitation is particularly evident for field-scale crop monitoring, where gathering ground truth data is tedious and rarely repeated throughout the growing season. Unsupervised learning methods, particularly clustering, offer a useful and efficient alternative in such data-constrained situations, allowing significant insight extraction without depending on labelled samples (Camps-Valls et al., 2013, Tuia et al., 2011). Clustering-based methods have shown great potential for identifying vegetation heterogeneity in agricultural landscapes by grouping data into clusters with similar spectral or temporal characteristics. Clustering makes it possible to identify zones with comparable crop vigor and growth trajectories when applied to vegetation indices like the Normalized Difference Vegetation Index (NDVI), which supports analysis of irrigation uniformity and management effectiveness (Peña-Barragán et al., 2011, Atzberger, 2013).

Graph-based and density-based approaches are two essentially distinct analytical paradigms among unsupervised clustering techniques. Instead of depending only on spatial proximity, spectral clustering is a graph-based method that divides data by examining pairwise similarities among pixels. Spectral clustering works well in high-dimensional feature spaces and can detect non-convex and irregular cluster structures by building a similarity graph and utilizing its spectral properties. This is especially useful for regions with heterogeneous vegetation (Shi and Malik, 2000, von Luxburg, 2007, Wang et al., 2024). In remote sensing tasks like image segmentation and spatial structure analysis, where relationships between pixels capture more information than their physical arrangement, graph-based clustering techniques have been widely used (Shi and Malik, 2000). For example, Saraiva et al. (Saraiva et al., 2020) showed how machine learning and remote sensing can be combined to automatically map centre-pivot irrigation systems, highlighting the significance of structural and pixel-level analysis in precision agriculture.

On the other hand, density-based clustering algorithms, like OPTICS, use local data density instead of global similarity to identify clusters. OPTICS allows for the detection of clusters with different densities without the need for a single distance threshold by ordering points based on their reachability distance (Ankerst et al., 1999). For NDVI-based agricultural imagery, where crop growth, soil moisture, and vegetation density vary significantly over time and space, this characteristic makes OPTICS especially appropriate (Kavita and Mathur, 2021). The usefulness of NDVI time-series when combined with machine learning techniques for adaptive agricultural monitoring and policy frameworks has been further shown by Lebrini et al.

(Lebrini et al., 2020). Moreover, Wu et al. (Wu et al., 2023) emphasized the need for robust algorithms capable of adapting to multi-scale spatial heterogeneity and temporal variability in remote sensing–based crop monitoring.

Graph and density approaches represent two fundamentally different analytical paradigms in unsupervised clustering. A significant research gap remains in systematically comparing these paradigms for crop growth analysis using multi-temporal NDVI data, despite the increasing number of studies that combine clustering methods with remote sensing.The majority of current research either concentrates on a single clustering technique or deep learning-based classification approaches. There are limited studies on clustering-based approaches for irrigation-driven crop growth variability and temporal stability.

Therefore, this study focuses on a comparative evaluation of spectral clustering and OPTICS for unsupervised clustering of multi-temporal NDVI imagery derived from centre-pivot irrigated agricultural fields. Understanding whether identified vegetation clusters stay constant or change over growth stages is important because this behaviour sheds light on the efficiency and consistency of irrigation techniques. This work contributes methodological insights to the remote sensing and data science communities while offering evidence-based recommendations for choosing suitable clustering techniques for precision agriculture applications through a systematic analysis of algorithm behaviour and cluster evolution over time.

2. Dataset

Satellite-derived NDVI data were used to analyse spatial and temporal variations in crop growth within irrigated fields.

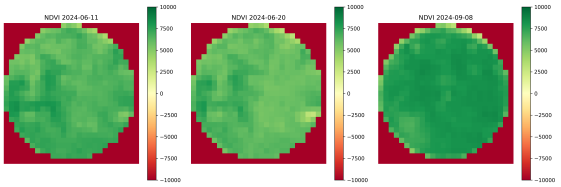

Figure 1. Field 1 (full center-pivot geometry) corresponding to NDVI acquisitions on 11 June 2024, 20 June 2024, and 8 September 2024. Green pixels represent the cultivated field area retained for analysis, while red pixels indicate background regions excluded from clustering and statistical evaluation.

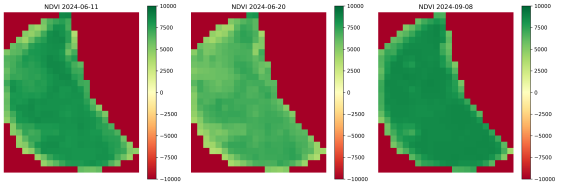

Figure 2. Field 2 (half-pivot geometry) corresponding to NDVI acquisitions on 11 June 2024, 20 June 2024 and 8 September 2024. The irregular field boundary introduces geometric asymmetry, providing a contrasting case for evaluating clustering robustness under non-circular field shapes

Date 1: June 11, 2024 – Early to mid-season crop development stage,representing initial canopy development and vegetative growth following planting. Average NDVI value was about 0.66 for field 1 and 0.72 for field 2.

Date 2: June 20, 2024 – Mid-season vegetative growth stage, characterized by rapid biomass accumulation and canopy closure. Average NDVI value was about 0.61 for field 1 and 0.63 for field 2.

Date 3: September 8, 2024 – Late season or senescence stage, representing crop maturity, harvest preparation, or post-harvest conditions. Average NDVI value was about 0.77 for field 1 and 0.79 for field 2.

2.1 Geographic Context

The study area is in southeastern Wyoming, USA, a semi-arid agricultural region characterized by centre-pivot irrigation systems that enable crop production in water-limited environments as shown in Figure 1 and Figure 2. The area has a continental climate with warm summers and frigid winters, with springtime seeing the most precipitation. Moderate temperatures (20–30°C) and low humidity are typical summer growing season conditions, and crop production depends on irrigation.The cultivated crop in both fields is Alfalfa hay, grown primarily as fodder.

In addition to shaping characteristic spatial patterns of crop growth linked to irrigation uniformity, soil variability, and topography, centre-pivot irrigation systems generate distinctive circular field patterns that are clearly visible in satellite imagery (Figure 1). Their geometric regularity and relatively uniform management practices within individual fields make them particularly well suited for remote sensing analysis.

2.2 Field Characteristics

For analysis, two agricultural fields with dissimilar geometries were chosen:
Field 1 (Full pivot): Figure 1 shows a full circular field that depicts a typical centre-pivot irrigation system with a consistent water distribution from a central point in all directions. The field displays typical centre-pivot system characteristics, such as edge effects close to field boundaries and possible variations in water application rates along the pivot arm length.

Field 2 (Half pivot): Figure 2 shows a semi-circular field that depicts a partial centre-pivot system and may be limited by water availability, property lines, or topographic features. Compared to complete circular systems, this field geometry adds spatial complexity and may show variability related to boundaries and edge effects.

By choosing fields with distinct geometries, generalizability of the chosen algorithm can be evaluated effectively.

2.3 Data Characteristics

Spatial Resolution: The 30-meter pixel size keeps data volumes manageable for computational analysis while offering enough spatial detail to describe within-field variability. Radiometric Resolution: 12-bit radiometric resolution (Landsat 8) makes it possible to distinguish minute variations in spectral reflectance linked to changes in crop health.

NDVI Representation: NDVI values were obtained directly from satellite-derived NDVI products. The NDVI data were provided in scaled integer format and were rescaled to the standard range of -1 to $+1$ prior to analysis.

The NDVI scale goes from -1 to $+1$, with the vegetated areas usually having values between 0.2 and 0.8. Greater vigour, density, and photosynthetic activity of the vegetation are indicated by higher values.

3. Methodology

3.1 Data Preprocessing

Preprocessing is a critical step in multi-temporal remote sensing analysis, as raw satellite-derived indices may contain noise, missing values, and scale inconsistencies that can bias clustering outcomes. The preprocessing procedures used on the NDVI datasets before feature construction and clustering are explained in the ensuing subsections.

The NDVI values from each date were loaded from precomputed raster datasets. To guarantee optimal radiometric fidelity, all NDVI rasters were loaded into a two-dimensional NumPy array(Harris et al., 2020) and processed with 32-bit floating-point precision.

No-data and invalid data region handling: NaN markers were programmatically used to replace "no data" values in the NDVI rasters, automatically masking and eliminating pixels unsuitable for clustering-such as non-vegetated, water, soil, or invalid NDVI pixels.

3.2 Feature Space Construction

Feature space construction is an important step in any unsupervised learning task, as it defines how raw data is represented for analysis. An effective feature representation is important for capturing vegetative changes rather than individual image situations in the context of multi-temporal NDVI research.

The main goal of this feature space is to depict each pixel's temporal growth behaviour over many acquisition dates as well as to its vegetation state on a single date. Pixels with similar patterns which includes steady growth, delayed growth, or stress-induced decrease that can be grouped together using clustering algorithms due to this representation.

3.2.1 Multi-Temporal Feature Vector

NDVI values from all three acquisition dates were stacked to create a multi-temporal feature vector for each pixel inside the field boundaries. Using this method, a three-dimensional feature space is produced, with each pixel represented as shown in equation 1
Feature Vector:

$$x_i = [NDVI_1, NDVI_2, NDVI_3]^T \tag{1}$$

where $NDVI_1$, $NDVI_2$, and $NDVI_3$ correspond to NDVI values on June 11, June 20, and September 8, respectively.

By capturing not only the current vegetation conditions but also phenological patterns and growth dynamics, this representation makes it possible for clustering algorithms to find pixels with comparable temporal trajectories of crop growth.

3.2.2 Feature Scaling and Standardization

Since NDVI values at different dates may exhibit varying ranges and distributions, direct use of raw features can bias distance-based similarity calculations.

Z-score normalization was applied to normalize feature vectors so that each time observation contributes equally to the clustering process as shown in equation 2

$$z = \frac{x - \mu}{\sigma} \tag{2}$$

Where μ and σ are the mean and standard deviation which are calculated for each temporal attribute in all pixels.

Due to this standardization, the result of clustering is not at all dominated by NDVI observations from a specific date with a larger numerical range.As a result, equal weight is assigned to all temporal dimensions, allowing the clustering algorithm to emphasize relative temporal patterns rather than absolute value differences.

3.2.3 Dimensionality and Feature Space Properties

Using one dimension for each date, the resulting 3-dimensional feature space accurately finds a balance between computational efficiency and representation depth. For large-scale pixel level analysis, this dimensionality is able to capture important crop growth patterns while retaining interpretability.

Additionally, the associations between temporal NDVI features have been shown to be mostly positive ($r = 0.4$–0.7) between consecutive dates. This shows that crop growth patterns show temporal consistency while maintaining sufficient independent data to support a multi-temporal analysis. These results verify that, in comparison to single-date NDVI representations, the provided feature space captures temporal variances.

3.3 Spectral Clustering Algorithm

3.3.1 Theoretical Foundation

By building a similarity graph $G = (V, E)$, where vertices V represent data points (pixels) and edges E encode pairwise similarities, Spectral clustering turns the clustering problem into a graph partitioning problem. The core idea behind this spectral clustering is that intrinsic clustering structure that might not be visible in the original feature space is revealed by the eigenvectors of graph-derived matrices, especially the graph Laplacian. The following conceptual steps are used by the algorithm to function:

1. Similarity Graph construction: Determine the similarity s_{ij} for every pair of pixels i and j using the feature space distance.
2. Laplacian graph Calculation: Create the Laplacian matrix for the normalized graph that represents graph connectivity.
3. Eigen decomposition: Compute eigenvalues and eigenvectors of the Laplacian matrix.
4. Spectral Embedding: Project data into lower-dimensional space spanned by leading eigenvectors
5. Final Clustering: Apply K-means or similar algorithm to clustered embedded representations.

3.3.2 Implementation Details

Similarity Matrix Construction: The Gaussian (RBF) kernel was employed to compute pairwise similarities between pixels as shown in Equation 3

$$s_{ij} = \exp\left(-\frac{\|x_i - x_j\|^2}{2\sigma^2}\right) \tag{3}$$

where $\|x_i - x_j\|^2$ represents the squared Euclidean distance between feature vectors in the standardized multi-temporal feature space, and σ is a scale parameter that controls the influence radius of each point.

The scale parameter σ was set using the median pairwise distance heuristic, which provides the robust similarity scaling without requiring manual tuning. This approach ensures that the similarity matrix captures meaningful local and global relationships while being robust to outliers.

Graph Laplacian Selection: The normalized symmetric graph Laplacian was employed as given in Equation 4

$$L_{sym} = I - D^{-1/2} W D^{-1/2} \tag{4}$$

where W is the similarity (affinity) matrix, D is the degree matrix (diagonal matrix with $D_{ij} = \sum_j W_{ij}$), and I is the identity matrix. The normalized Laplacian provides better numerical stability and theoretical properties compared to the unnormalized Laplacian.

Eigen decomposition: The leading k eigenvectors (corresponding to the k smallest eigenvalues) of the graph Laplacian were computed using efficient sparse matrix algorithms. These eigenvectors form a new representation where clusters are more separable.

Cluster Assignment: K-means clustering was applied to the rows of the eigenvector matrix, with multiple random initializations ($n = 10$) to avoid local optima and ensure reproducible results.

Together, these processes convert the initial multi-temporal pixel space into a graph-based embedding that explicitly captures the structural relationships between pixels. By effectively projecting pixels into a space where regions with similar temporal behavior become closely packed, the eigenvectors of the normalized Laplacian provide a low-dimensional representation that maintains the intrinsic geometry of the data. Since pixels with comparable growth trajectories are grouped together, applying K-means in this spectral domain results in clusters that correspond to coherent vegetation regions. The method may shift from raw NDVI measurements to spatially consistent, semantically meaningful field segments driven by shared temporal dynamics because of to this eigen-to-cluster transition.

3.3.3 Cluster Number Determination: Eigengap Heuristic

A critical challenge in Spectral clustering is determining the optimal number of clusters k. The eigengap heuristic provides a principled approach based on the eigenvalue spectrum of the graph Laplacian.

The eigengap is defined as the difference between consecutive eigenvalues as shown in Equation 5

$$gap_i = \lambda_{i+1} - \lambda_i \tag{5}$$

A large eigengap indicates a natural separation in the spectral structure, suggesting that i clusters provide an appropriate partition of the data. The optimal k is selected as given in Equation 6

$$k^* = \arg\max_i (gap_i) \tag{6}$$

For this study, eigenvalue spectra were computed for k ranging from 2 to 15 clusters, and eigengap values were visualized to identify the most pronounced gap. This analysis consistently identified $k = 4$ or $k = 5$ as optimal for the agricultural fields analysed, corresponding to interpretable vegetation zones with distinct growth patterns.

3.4 OPTICS Clustering Algorithm

This section describes the theoretical background, the key parameters, and the implementation details of the OPTICS algorithm as applied in this study. The description below focuses on the concepts and design choices relevant to multi-temporal NDVI-based agricultural analysis, while detailed comparative results are presented in subsequent sections.

3.4.1 Theoretical Foundation

OPTICS extends DBSCAN (Kanagala and Krishnaiah, 2016) by capturing hierarchical density structures instead of producing a single clustering solution. This capability allows it to detect both large-scale field zones and localized micro-variability in NDVI imagery.

The algorithm relies on two main concepts:
Core Distance (CD): The minimum radius required for a point to have at least min_samples neighbors. In NDVI maps, high NDVI regions (≈ 0.6676 in Field 1 on June 11, 2024) form dense cores with small CD values, while low NDVI areas (≈ 0.25–0.50 during senescence) form sparser clusters with larger CDs.
Reachability Distance (RD): The minimum distance at which a point can be reached from another, given the core distance. RD reflects transitions between vegetation zones, highlighting edges, micro-stress patches, or isolated high-vigor areas.

OPTICS uses these measures to produce an augmented ordering and a reachability plot, where valleys correspond to dense clusters and peaks indicate sparse regions or noise. This structure allows flexible cluster extraction at multiple density levels, making OPTICS well-suited for identifying both stable field-scale zones and fine-scale anomalies in NDVI data.

3.4.2 Key Parameters

The main parameters controlling OPTICS clustering are:
min_samples: Minimum number of points in a neighborhood for a point to be considered a core point. Smaller values allow detection of fine-grained clusters, larger values focus on dominant dense zones.
max_eps: Maximum neighborhood radius for computing thereachability distances, controlling the scale of cluster detection.
xi: Steepness threshold in the reachability plot used to define cluster boundaries. Smaller xi detects subtle density changes, larger xi identifies only major clusters.

In this study, these parameters were systematically explored to balance detection of micro-variability and field-scale zones.

3.4.3 Implementation Details

Distance Metric: To ensure a fair comparison with spectral clustering, Euclidean distance was computed in the standardized three-dimensional multi-temporal NDVI feature space. This ensures that each temporal NDVI component contributes equally to the distance computation, preventing bias toward any single

acquisition date.

Reachability Plot Computation: OPTICS algorithm iteratively processes points by expanding dense regions and updating the reachability distances of neighboring points, thereby producing an ordered list of observations. A reachability plot, defined as reachability distance versus OPTICS ordering, provides a visual representation of the hierarchical density structure present in the data. In this plot, valleys correspond to dense clusters, while peaks indicate transitions between clusters or sparse regions, including noise.

Figure 3 presents a reachability plot generated for the NDVI dataset from field 1, dated 08-09-2024, clearly illustrating this density-based organization.

Cluster Extraction (xi Method): Clusters were directly extracted from the reachability plot using the xi method. This approach identifies clusters by detecting steep downward transitions, which signify entry into dense regions, and steep upward transitions, which indicate exit from these regions. The sensitivity of cluster detection is controlled by the xi parameter, which defines the minimum relative steepness required to identify meaningful cluster boundaries. This enables robust identification of clusters across varying density levels without explicitly specifying the number of clusters a priori.

Noise Handling and Outer Regions: Points exhibiting consistently high reachability distances, particularly those appearing at the outer regions of the reachability plot, are automatically classified as noise. These outer regions represent low-density areas where observations cannot be reliably assigned to any dense cluster. As shown in Figure 3 the elevated reachability distances at the beginning and end of the ordering correspond to such low-density or transitional regions. This inherent noise detection capability is a key advantage of OPTICS over partition-based clustering methods, as it allows outliers and ambiguous observations to be handled naturally without forced assignment.

Reachability Plot Visualization: The reachability plot shown in Figure 3 (logarithmic scale) is included to visually demonstrate the relationship between reachability distance, cluster density, and noise. Dense vegetation clusters appear as pronounced valleys, while cluster boundaries and noise-dominated outer regions manifest as peaks with high reachability distances.

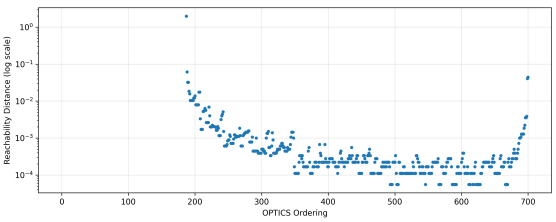

Figure 3. OPTICS reachability plot (logarithmic scale) for the 2024-09-08 NDVI dataset, illustrating dense vegetation clusters as valleys and outer regions with high reachability distances corresponding to noise and low-density transitions between clusters.

3.4.4 Parameter Tuning Strategy

To enable a fair comparison with Spectral clustering, OPTICS parameters were systematically tuned through a three-phase approach:
(a) a broad exploration of parameter ranges (min_samples: 3–25, xi: 0.005–0.5) was conducted to characterize algorithm behaviour and identify feasible settings;
(b) refinement then focused on parameter combinations yielding 4–8 clusters, consistent with the number of clusters produced by Spectral clustering; and
(c) final fine-tuning optimized cluster spatial coherence and interpretability while maintaining consistent cluster counts.

This systematic procedure identified an optimal configuration of min_samples = 5 and xi = 0.035. This configuration balances sensitivity to local density variations while producing spatially interpretable clusters and cluster counts comparable to those obtained using Spectral clustering, thereby enabling a meaningful comparison of clustering paradigms rather than a comparison driven solely by differences in cluster granularity.

4. Results and Discussions

This section presents and discusses the key spatial and temporal patterns observed in the NDVI-based clustering results, building upon the methodology described in the preceding sections.

4.1 Insights from Field 1

Figure 4 illustrates the spatial clustering outcomes for Field 1 across three NDVI acquisition dates (11 June 2024, 20 June 2024, and 8 September 2024), obtained using Spectral Clustering (top row) and OPTICS (middle row), along with the corresponding Intersection-over-Union (IoU) matrices (bottom row). For each date, cluster 0 denotes background or masked pixels excluded from vegetation analysis, while the remaining clusters represent distinct vegetation growth zones.

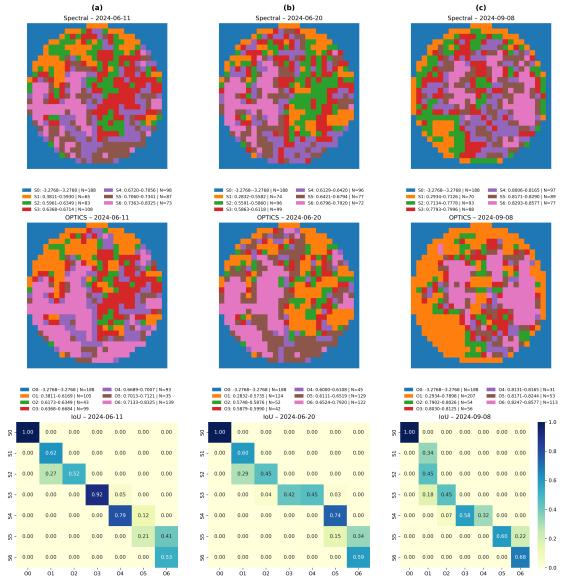

Figure 4. Spatial clustering results for Field 1 across three NDVI acquisition dates (11 June 2024, 20 June 2024, and 8 September 2024) using Spectral Clustering (top row) and OPTICS (middle row), together with the corresponding Intersection-over-Union (IoU) matrices (bottom row).

(a) June 11, 2024 (Early Growth Stage): At the beginning of the growing season, both Spectral (S) and OPTICS (O) clustering results exhibit a clear circular spatial organization consistent with center-pivot irrigation patterns (Fig. 4). In the Spectral clustering map, seven smooth and radially ordered zones are observed, with the high-vigor central area represented by pink and light-violet clusters (S), which gradually transition outward into moderate and low-vigor zones shown in orange, green, and red (S). These zones form spatially cohesive, field-scale management regions with well-defined boundaries.

The OPTICS result preserves this overall radial gradient while introducing finer spatial detail. Within the central high-vigor region, isolated high-NDVI pockets (pink, O) are visible, whereas along the field boundary, small dispersed clusters in dark-red and green (O) appear. Additionally, narrow linear features aligned with irrigation tracks are evident as bands of contrasting colors (O). These patterns indicate early-stage micro-heterogeneity and localized variability captured by OPTICS, in contrast to the stable and interpretable zones identified by Spectral clustering.

(b) June 20, 2024 (Peak Vegetative Growth): During peak vegetative growth, both clustering approaches indicate active canopy development across the field (Fig. 4). The Spectral clustering result highlights a structured, field-scale expansion pattern, where the surrounding moderate- and low-vigor zones (orange, green, and red clusters, S) shift outward, while the high-vigor central region (pink and light-violet clusters, S) expands radially. This organized spatial evolution reflects uniform crop development under center-pivot irrigation.

The OPTICS map retains the same hierarchical structure but exhibits increased spatial complexity. Numerous small micro-clusters in green, red, and orange (O) appear throughout mid-field and peripheral areas, suggesting localized variations possibly related to soil heterogeneity, uneven water distribution, or early stress conditions. While Spectral clustering emphasizes coherent, large-scale growth dynamics, OPTICS reveals subtle deviations from spatial uniformity, with both methods remaining consistent in their depiction of overall growth trends.

(c) September 8, 2024 (Late Season / Senescence): By the late season, both Spectral and OPTICS results demonstrate a pronounced decline in NDVI values (approximately 0.25–0.50), indicative of crop senescence, while preserving the relative spatial ordering of vegetation zones (Fig. 4). The Spectral clustering map continues to display large, coherent regions, with senescent and low-vigor zones primarily shown in orange and green (S), and comparatively higher-vigor central areas still represented by broad pink and light-violet clusters (S). This persistence suggests that underlying spatial controls, such as soil properties, field position, and irrigation distribution, continue to influence vegetation patterns beyond peak growth.

In contrast, the OPTICS result shows marked spatial fragmentation. Small residual regions of green and pink (O) are scattered within predominantly orange senescent areas, highlighting localized persistence of vegetation and staggered senescence or harvest progression. These fine-scale residual patterns, which are merged into larger zones in the Spectral result, demonstrate the heightened sensitivity of OPTICS to micro-level variability during late-season dynamics.

Insights from Stacked Image for Field 1

The Spectral Clustering result (left, S), derived from the stacked multi-temporal NDVI feature space (Fig. 5), delineates seven

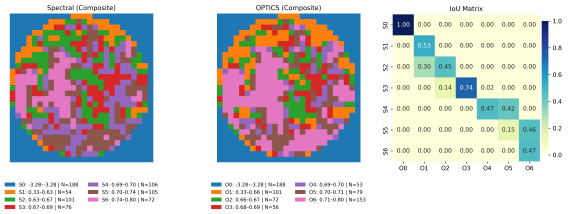

Figure 5. Clustering results for Field 1 obtained from the compiled multi-temporal NDVI feature space using Spectral Clustering and OPTICS, along with the corresponding IoU matrix.

highly stable, radially organized vegetation zones that persist across the growing season. These cohesive and smooth regions, dominated by lower-vigor orange and green clusters (S) toward the margins and persistent high-vigor pink and light-violet clusters (S) at the center, reflect long-term productivity patterns created by integrating all acquisition dates rather than single-date variability. The OPTICS result (center, O) introduces finer sub-field distinction while maintaining the same macro-scale circular structure. Small green, red, and orange patches (O) embedded within larger regions indicate persistent micro-zones and localized anomalies, reflecting time-consistent local variability throughout the season.

The main core and mid-field regions in the IoU matrix (right, Fig. 5) show moderate-to-strong correspondence, whereas the outer and more heterogeneous areas show lower agreement.

This temporal integration highlights a key distinction: OPTICS remains sensitive to ongoing fine-scale variability, while Spectral clustering emphasizes stable, seasonal management regions. The stacking analysis demonstrates that combining multi-temporal data enhances the detection of persistent field structure while retaining the complementary strengths of density-based and global clustering techniques.

4.2 Insights from Field 2

Figure 6 illustrates the spatial clustering outcomes for Field 2 across three NDVI acquisition dates (11 June 2024, 20 June 2024, and 8 September 2024), obtained using Spectral Clustering (top row) and OPTICS (middle row), along with the corresponding Intersection-over-Union (IoU) matrices (bottom row). For each date, cluster 0 denotes background or masked pixels excluded from vegetation analysis, while the remaining clusters represent distinct vegetation growth zones.

(a) June 11, 2024 (Early Growth Stage): The half-pivot system's semi-circular configuration is captured by both Spectral (S) and OPTICS (O) clustering (Fig. 6). A distinct straight-edge boundary region (orange and green clusters, S), arc-shaped mid-field zones (red and orange clusters, S), low-vigor peripheral areas, and a high-vigor core near the pivot represented by pink and light-violet clusters (S) are clearly visible as smooth, geometry-aware zones in the Spectral map. These spatially coherent areas form distinct management zones aligned with field geometry and irrigation. This macro-scale pattern is preserved in the OPTICS output, although visible fragmentation occurs, particularly along the straight boundary. Early boundary-driven heterogeneity is revealed through linear features and small high-density patches appearing as dispersed green, red, and violet clusters (O). OPTICS thus highlights localized variability and edge effects even at the early growth stage, whereas Spectral clustering emphasizes cohesive and interpretable regions.

(b) June 20, 2024 (Peak Vegetative Growth): The high-vigor central region, represented by pink and light-violet clusters (S), expands outward in the Spectral result, while the surrounding zones (orange, red, and green clusters, S) shift smoothly, indicating ordered field-scale development and a consistent NDVI increase (Fig. 6). Along the straight boundary, a comparatively larger NDVI increase is observed (≈ 0.12 versus ≈ 0.08 elsewhere), suggesting delayed but accelerated growth in this edge region. The OPTICS map (O) highlights greater boundary-driven variability while maintaining the overall growth hierarchy. Several micro-clusters emerge as small green, red, and orange patches (O), particularly along the straight edge, resulting in six to seven distinct regions. While both methods agree on the overall upward growth trend, OPTICS reveals localized deviations, whereas Spectral clustering emphasizes structured and coherent development.

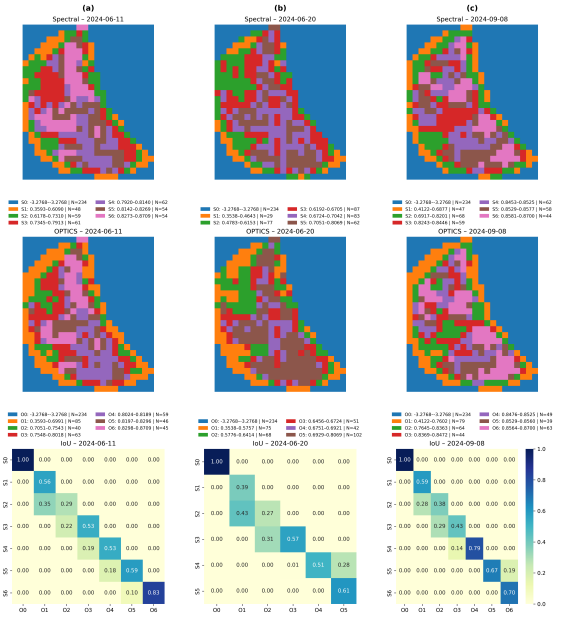

Figure 6. Spatial clustering results for Field 2 across three NDVI acquisition dates (11 June 2024, 20 June 2024, and 8 September 2024) using Spectral Clustering (top row) and OPTICS (middle row), together with the corresponding Intersection-over-Union (IoU) matrices (bottom row).

(c) September 8, 2024 (Late Season / Senescence): In the Spectral result (S), NDVI convergence leads to the merging of zones into three dominant, geometrically coherent regions, with broad light-violet and purple clusters in the interior and orange–green regions toward the periphery (Fig. 6). These smooth zones indicate that underlying spatial controls remain influential late in the season, reflecting varying senescence or harvest timing while preserving half-pivot geometry. In contrast, the OPTICS map (O) undergoes stronger restructuring, forming four to five major clusters along with additional noise regions that differentiate fully senescent areas from remaining green vegetation. Within predominantly orange senescent regions, small green and violet patches (O) persist, indicating isolated vegetation survival. This fragmentation, most pronounced near the straight boundary, highlights OPTICS' sensitivity to late-season micro-variability and boundary-driven heterogeneity.

Insights from Stacked Image for Field 2

The Spectral Clustering result (left, S), computed from the stacked multi-temporal NDVI feature space (Fig. 7),

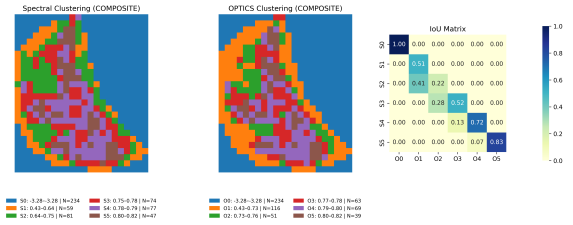

Figure 7. Clustering results for Field 2 obtained from the compiled multi-temporal NDVI feature space using Spectral Clustering and OPTICS, along with the corresponding IoU matrix.

delineates stable vegetation zones that naturally conform to the semi-circular geometry of the half-pivot field. These smooth, geometry-aware clusters reflect repeating productivity patterns influenced by boundary effects and irrigation design through seasonal integration. The OPTICS result (middle, O) introduces increased spatial fragmentation, particularly along geometric discontinuities and the straight boundary, while preserving the same macro-scale structure. Localized anomalies and time-consistent micro-zones appear as small green, red, and violet patches (O), emphasizing persistent fine-scale variability.

The central and mid-field regions exhibit moderate correspondence in the IoU matrix (right, Fig. 7), whereas the straight edge and peripheral areas show lower agreement. This indicates that while both methods capture irrigation-driven gradients over time, they respond differently to boundary-driven and local variability. Overall, the stacking analysis shows that OPTICS remains sensitive to persistent micro-scale variability amplified by irregular field geometry, whereas Spectral clustering prioritizes seasonally stable, geometry-respecting management regions.

5. Conclusion

This study establishes that graph-based and density-based clustering approaches provide complementary strengths for unsupervised analysis of multi-temporal NDVI in irrigated agricultural fields. Spectral clustering is well suited for strategic management zone delineation due to its ability to produce spatially coherent, interpretable zones that remain stable across the growing season. In contrast, OPTICS offers enhanced sensitivity to localized variability, making it particularly effective for identifying fine-scale anomalies and subtle heterogeneities in crop vigor. From an operational perspective, these differences highlight the importance of aligning algorithm selection with application objectives. Tasks requiring consistent, field-scale zoning and decision support benefit from Spectral clustering, whereas exploratory analyses and diagnostic monitoring are better served by OPTICS. Rather than viewing these methods as competing alternatives, the results support an integrated framework in which Spectral clustering informs long-term planning while OPTICS enables targeted, tactical interventions. More broadly, this work demonstrates that informed method selection and careful parameterization are critical for extracting actionable insights from Earth observation data. The proposed comparative framework can be extended to other unsupervised approaches and datasets, supporting scalable, data-driven crop monitoring strategies. Such integration of advanced machine learning with remote sensing holds significant potential for improving precision agriculture practices and promoting sustainable agricultural management.

References

Ankerst, M., Breunig, M. M., Kriegel, H.-P., Sander, J., 1999. OPTICS: Ordering points to identify the clustering structure. *SIGMOD Record*, 28(2), 49–60.

Atzberger, C., 2013. Advances in remote sensing of agriculture: Context description, existing operational monitoring systems and major information needs. *Remote Sensing*, 5(2), 949–981.

Camps-Valls, G., Tuia, D., Bruzzone, L., Benediktsson, J. A., 2013. Advances in hyperspectral image classification: Earth monitoring with statistical learning methods. *IEEE Signal Processing Magazine*, 31(1), 45–54.

Harris, C. R., Millman, K. J., van der Walt, S. J. et al., 2020. Array programming with NumPy. *Nature*, 585, 357–362.

Kanagala, H. K., Krishnaiah, V. V. J. R., 2016. A comparative study of k-means, dbscan and optics. *2016 International Conference on Computer Communication and Informatics (ICCCI)*.

Kavita, Mathur, P., 2021. Satellite-based crop yield prediction using machine learning algorithm. *Asian Conference on Innovation in Technology (ASIANCON)*, 1–5.

Lebrini, Y., Boudhar, A., Htitiou, A., Hadria, R., Lionboui, H., Bounoua, L., Benabdelouahab, T., 2020. Remote monitoring of agricultural systems using NDVI time series and machine learning methods: A tool for an adaptive agricultural policy. *Arabian Journal of Geosciences*, 13(16), 796.

Peña-Barragán, J. M., Ngugi, M. K., Plant, R. E., Six, J., 2011. Object-based crop identification using multiple vegetation indices, textural features and crop phenology. *Remote Sensing of Environment*, 115(6), 1301–1316.

Saraiva, M., Protas, E., Salgado, M., Souza, C., 2020. Automatic mapping of center pivot irrigation systems from satellite images using deep learning. *Remote Sensing*, 12(3), 558.

Shi, J., Malik, J., 2000. Normalized cuts and image segmentation. *IEEE Transactions on Pattern Analysis and Machine Intelligence*, 22(8), 888–905.

Tuia, D., Volpi, M., Copa, L., Kanevski, M., Muñoz-Marí, J., 2011. A survey of active learning algorithms for supervised remote sensing image classification. *IEEE Journal of Selected Topics in Signal Processing*, 5(3), 606–617.

von Luxburg, U., 2007. A tutorial on spectral clustering. *Statistics and Computing*, 17, 395–416.

Wang, J., Wang, Y., Qi, Z., 2024. Remote sensing data assimilation in crop growth modeling from an agricultural perspective: New insights on challenges and prospects. *Agronomy*, 14(9), 1920.

Wu, B., Zhang, M., Zeng, H., Tian, F., Potgieter, A. B., Qin, X., Yan, N., Chang, S., Zhao, Y., Dong, Q., Boken, V., Plotnikov, D., Guo, H., Wu, F., Zhao, H., Deronde, B., Tits, L., Loupian, E., 2023. Challenges and opportunities in remote sensing-based crop monitoring: A review. *National Science Review*, 10(4), nwac290.